Korea-Australia Rheology Journal
Vol. 20, No. 3, September 2008 pp. 165-173

Hydrogel microrheology near the liquid-solid transition

Travis Larsen, Kelly Schultz and Eric M. Furst*
Department of Chemical Engineering and Center for Molecular and Engineering Thermodynamics, University of Delaware, Newark, DE 19716

(Received May 21, 2008)

Abstract

Multiple particle tracking microrheology is used to characterize the viscoelastic properties of biomaterial and synthetic polymer gels near the liquid-solid transition. Probe particles are dispersed in the gel precursors, and their dynamics are measured as a function of the extent of reaction during gel formation. We interpret the dynamics using the generalized Stokes-Einstein relationship (GSER), using a form of the GSER that emphasizes the relationship between the probe particle mean-squared displacement and the material creep compliance. We show that long-standing concepts in gel bulk rheology are applicable to microrheological data, including time-cure superposition to identify the gel point and critical scaling exponents, and the power-law behavior of incipient network's viscoelastic response. These experiments provide valuable insight into the rheology, structure, and kinetics of gelling materials, and are especially powerful for studying the weak incipient networks of dilute gelators, as well as scarce materials, due to the small sample size requirements and rapid data acquisition.

Keywords : hydrogel, peptide, microrheology, particle tracking, superposition, critical gel

1. Introduction

New synthetic biomaterials that assemble or self-assemble to form hydrogel networks are of great interest for numerous therapeutic applications. Such hydrogelators have shown exciting potential for use in wound healing, drug delivery, and tissue engineering (Ellis-Behnke *et al.*, 2006; Davis *et al.*, 2005; Grinstaff, 2007; Peppas *et al.*, 2000; Hoffman, 2002; Langer and Peppas, 2003; Lee and Mooney, 2001; Rajagopal and Schneider, 2004; Lutolf and Hubbell, 2005; Stevens and George, 2005). For biomaterials, characterizing the evolution of the micro-scale viscoelastic properties, structure, degree of heterogeneity, and kinetics of network formation through the liquid-solid (sol-gel) transition is particularly important. For instance, cell encapsulation in a three-dimensional hydrogel network is important for tissue engineering and wound healing applications because it improves cell proliferation and tissue organization when compared to growth on a two-dimensional surface. However, biological properties such as cell attachment and mobility, nutrient transport, and suspension homogeneity are dependent on the material structure and elasticity (Mikos *et al.*, 2006; Davis and Vacanti, 1996), porosity (Chin and Vacanti, 2008; Wu *et al.*, 2008), and gelation kinetics (Haines-Butterick *et al.*, 2007), respectively. Thus, microrheology, in which the thermal motion of dispersed microspheres is used to probe the material rheology, has been increasingly applied to study these hydrogelators (Tseng *et al.*, 2002; Gardel *et al.*, 2003; Xu *et al.*, 2005; Veerman *et al.*, 2006; Zimenkov *et al.*, 2006; Savin and Doyle, 2007).

There are several advantages for using microrheology to study hydrogelators. The initial stages of gelation are often rapid, and the mechanical properties of the incipient networks are weak. Microrheology provides sensitivity to the viscoelastic properties at lower moduli (≤ 5 Pa), while also providing the ability to measure several decades of timescales (1 ms – 10 s) with short measurement acquisition times (~30 sec). Microrheology typically requires small sample volumes (<50 μL), which makes it possible to investigate the rheological properties of scarce materials. Microrheology also minimizes the risk of disturbing the fragile microstructure as it develops, since external forces are not applied. Despite the importance of microrheology for characterizing these emerging biomaterials, methods for determining key physical characteristics of the liquid-solid transition have only recently been reported by Larsen and Furst (2008).

Before discussing microrheology near the liquid-solid transition in greater detail, we first review the physical characteristics of gelation. The liquid-solid transition is similar to a continuous thermodynamic phase transition. Gelation exhibits critical behavior, including a critical

*Corresponding author: furst@udel.edu

point (the gel point), the divergence of certain physical properties, and scaling behavior near the gel point. The critical gel point is defined as the extent of reaction p at which the first percolating cluster spans the sample-space, p_c. Rheological properties, such as the zero shear viscosity η_0, equilibrium compliance J_e^0 and longest relaxation time τ_L, diverge at the critical gel point (Stauffer *et al.*, 1982; Joanny, 1982). Defining the extent of reaction, or distance from the gel point, as $\varepsilon \equiv |p-p_c|/p_c$, the scaling relationships are $\eta_0 \sim \varepsilon^{-k}$, $J_e^0 \sim \varepsilon^{-z}$ and $\tau_L \sim \varepsilon^{-y}$, where k, z and y are critical scaling exponents (Stauffer *et al.*, 1982; Martin *et al.*, 1988; 1989; Adolf and Martin, 1990). These scaling exponents are not independent, but are related by $y=k+z$ (Adolf and Martin, 1990).

The critical scaling behavior near the gel point results in an unusual feature of gels, first identified by Winter and Chambon (1986; 1987): at the gel point, the viscoelastic moduli of the incipient network exhibit power-law scaling with frequency $G' \sim G'' \sim \omega^n$. The critical relaxation exponent n is related to the critical exponents of the compliance and longest relaxation time by the scaling relationship $n=z/y$.

In bulk rheology, monitoring the loss tangent $\tan\delta = G''/G'$ of a material as a function of the extent of gelation provides a more robust method for identifying the gel point than measurements of diverging properties, such as the viscosity, relaxation time or compliance (Winter and Chambon, 1986; 1987; Winter and Mours, 1997; Scanlan and Winter, 1991). The gel point and relaxation exponent provide valuable information about the gelation kinetics and characteristics of the network connectivity (Scanlan and Winter, 1991).

Unfortunately, accurate measurements of $\tan\delta$ can be difficult using microrheology. To understand why, consider that microrheology relates the ensemble averaged mean-squared displacement (MSD) of embedded probes to the viscoelastic properites of the material by the generalized Stokes-Einstein relation (GSER),

$$\langle \Delta \tilde{r}^2(s) \rangle = \frac{2k_BT}{\pi D s \tilde{G}(s)} \tag{1}$$

where D is the probe particle diameter, $\tilde{G}(s)$ is the Laplace transform of the relaxation modulus and $\langle \Delta \tilde{r}^2(s) \rangle$ is the Laplace transform of the mean-squared displacement. While the viscoelastic moduli can be determined from Eq. (1), doing so involves approximations or numerical transformations of the discrete data that introduce noise, resulting in a sometimes ambiguous interpretation of $\tan\delta$ (Mason, 2000). Eq. (1) also requires a sufficient range of timescales or frequencies, which is sometimes not possible to obtain, for instance, when the material is gelling quickly or the dynamics are subject to static and dynamic errors at short lag times (Bobroff, 1986; Savin and Doyle, 2005).

We recently showed that it is possible to identify the gel point, critical relaxation exponent, and dynamic scaling exponents of hydrogels directly from the mean-squared displacement data obtained in microrheology (Larsen and Furst, 2008). Our approach relies on the direct relationship between the creep compliance $J(\tau)$ and the MSD. Specifically, using the relationship between the Laplace transforms of the creep compliance and the relaxation modulus $J(s)=1/s\tilde{G}(s)$ (Ferry, 1980), the GSER can be rewritten as (Palmer *et al.*, 1998)

$$J(\tau) = \frac{\pi D}{2k_BT} \langle \Delta r^2(\tau) \rangle . \tag{2}$$

More intuitively, the probe particle motion in microrheology is a measure of the strain deformation ($\langle \Delta r^2(\tau) \rangle / a^2$) that results from the average thermal stress imparted on the bead ($\sim k_BT/a^3$). At the gel point, the MSD and creep compliance exhibit power-law behavior over all times

$$J_c(\tau) = \frac{\sin n\pi}{n\pi S} \tau^n \tag{3}$$

where S is the gel strength and n is the critical relaxation exponent (Joanny, 1982; Winter and Chambon, 1986; 1987). Near the gel point, $J(\tau)$ can be shifted to generate master curves by plotting $b\langle \Delta r^2(\tau) \rangle$ versus $a\tau$. The a, accounts for the change in longest relaxation time, $a \sim \tau_L^{-1} \sim \varepsilon^y$, while the vertical shift factor, b, accounts for the change in the equilibrium compliance, $b \sim 1/J_e^0 \sim \varepsilon^z$. The expected behavior of the probe particle mean-squared displacement is shown in Fig. 1 in terms of the equivalent creep compliance. As we will show in this paper, the diver-

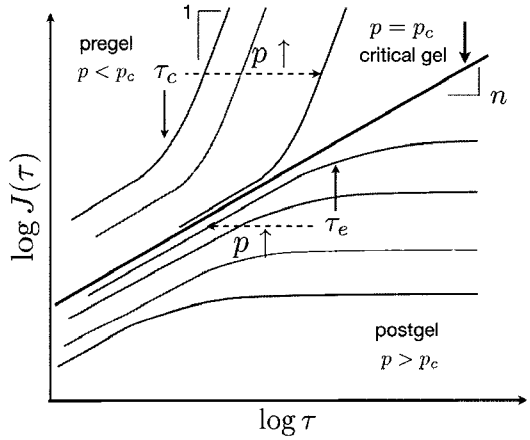

Fig. 1. Expected behavior of the mean-squared displacement of probe particles in the vicinity of the liquid-solid transition. The longest relaxation time in the pregel τ_c increases with increasing extent of reaction. The corresponding longest relaxation time in the postgel τ_e decreases with extent of reaction beyond the gel point. At the gel point, the compliance (MSD) scales as $J_c \sim \tau^n$, where n is the critical relaxation exponent. $J(\tau)$ decreases throughout the gelation process.

gence of the reciprocal values of the shift factors, a^{-1} and b^{-1}, near the sol-gel transition can be used to determine the gel point, p_c. The critical exponents, y, z and n are then obtained from the scaling of the shift factors as a function of the distance from the gel point, ε.

Our aim here is to compare microrheology data from several materials as they pass through the sol-gel transition. The first material we discuss is a peptide hydrogel that undergoes a dynamic, time-dependent sol-gel transition; thus, the extent of reaction is a function of time. We compare this to equilibrated, covalently cross-linked networks with a well-defined extent of cross-linking. The first covalent system is polyacrylamide. The second covalently cross-linked material is composed of maleimide-functionalized high molecular weight heparin and a bis-thiol PEG cross-linker. Before discussing our results, we detail the experimental methods used in this work. We conclude the paper with key observations of successes and limitations in applying microrheology to characterize the gel transition.

2. Experimental section

Materials. The 20-residue peptide MTHR (VKVKVKV KV^{D}PPTKVTVKVKV-NH_2) consists of an alternating sequence of valine and lysine residues flanking a central tetrapeptide sequence with a high β-turn propensity. MTHR is identical to the previously described parent peptide MAX1, with a single amino acid substitution at the 15th residue position, which replaces a lysine with a threonine (K15T) (Pochan *et al.*, 2003). Gelation of this peptide is designed to be responsive to changes in the environmental conditions. Increasing the pH or ionic strength reduces or screens the repulsive forces between positively-charged lysine residues, triggering the peptide to assemble into a highly cross-linked β-hairpin-rich filamentous network (Schneider *et al.*, 2002; Pochan *et al.*, 2003; Ozbas *et al.*, 2004). The synthesis and purification of the peptide follows standard solid-phase fmoc protocols, as described in detail elsewhere (Pochan *et al.*, 2003).

Chemically cross-linked polyacrylamide is a polymeric gel that forms via the free-radical polymerization of acrylamide monomers. Cross-linking between polymer molecules is induced by the addition of bis-acrylamide, a covalently-linked acrylamide dimer that randomly incorporates into growing filaments during polymerization. The extent of reaction is directly proportional to the amount of bis-acrylamide. Therefore, equilibrated samples can be prepared at various points during the gelation process by varying the concentration of bis-acrylamide. The polymerization reaction is monitored using UV-vis spectroscopy to ensure adequate time (~6 hrs) is allowed for the samples to reach equilibrium conversion before measurements are taken. The acrylamide and bis-acrylamide are obtained from commercial suppliers (Sigma-Aldrich) and used as received without further purification.

The reaction of maleimide-functionalized high molecular weight heparin (HMWH) and bis-functional poly(ethylene glycol) (PEG) results in covalently cross-linked heparin-PEG hydrogels (HMWH-PEG). Heparin, a polysaccharide which is a glycosaminoglycan, is used as a backbone and functionalized with maleimide groups. The maleimide groups chemically bond with the terminal thiol groups of the poly(ethylene glycol). Data can be taken throughout the gelation process, capturing the hydrogel at various extents of reaction in time and composition. High molecular weight heparin is functionalized by dissolution of heparin sodium salt (Grade I-A from porcine intestinal mucosa, Sigma-Aldrich) in 2-(Nmorpholino) ethanesulfonic acid (MES, Sigma-Aldrich) buffer containing N-(3-dimethylaminopropyl)-N'-ethylcarbodimide hydrochloride (EDC-HCl, Sigma-Aldrich, 3 equivalents to COOH groups to HMWH), 1-hydroxybenzotriazole hydrate (HOBT, Sigma-Aldrich) or N-hydroxy succinimide (NHS, Sigma-Aldrich, 3 equivalents to COOH groups in HMWH) and N-(2-aminoethyl) maleimide (AEM, Sigma-Aldrich) (Nie *et al.*, 2007). The functionality of the HMWH is controlled by the pH of the reaction solution and is purified by dialysis and characterized using NMR (Nie *et al.*, 2007). A HMWH with 4.2 maleimide group functionality is used for kinetic studies. Poly(ethylene glycol) (Average M_n 10,000 g/mol, Sigma-Aldrich, 2 mmol OH groups) is dithiolized in a reaction mixture with mercaptopropionic acid (Sigma, Aldrich, 40 mmol), p-toluenesulfonic acid (Sigma-Aldrich, 0.4 mmol) and dithiothreitol (DTT, Sigma-Aldrich, 1 mmol) dissolved in toluene. The solution is refluxed with stirring over a period of 24 hours and percipitated in cold acid (Nie *et al.*, 2007). Hydrogels are made by dissolving the appropriate amount of HMWH and PEG separately in phosphate buffered saline (pH 7.4, Invitrogen Corp.).

Sample preparation–Microrheology samples are prepared in a similar manner for each reaction system. MTHR peptide gel samples are made by dispersing lyophilized peptide in water (conductivity 18.2 MΩ·cm) and then initiating gelation by adding buffer to increase the pH. The final sample contains 0.15 wt% peptide in pH 8.5 buffer (50 mM BTP).

Polyacrylamide samples are prepared at 3.0 wt% total acrylamide, 0.0 - 0.1 wt% bis-acrylamide cross-linker, 0.5 wt% ammonium persulfate initiator, and 0.1% TEMED catalyst. All materials are obtained commercially (Sigma-Aldrich), and stock solutions are made daily and degassed to remove dissolved oxygen, which is known to retard the polymerization reaction. HMWH-PEG gels are initiated by mixing of the two solutions of maleimide-functionalized HMWH and dithiol PEG. Fluorescent polystyrene tracer particles (D=1.05±0.01 μm, Polysciences, Warrington, PA) are washed three times, sonicated, and added to a final concentration of 0.15 v% before gelation is initiated.

Multiple particle tracking microrheology–Sample preparation procedures have been detailed previously (Larsen and Furst, 2008). Immediately after gelation is initiated, sample solutions are introduced into rectangular capillary cells (0.20×2.00×50 mm, Vitrotubes, Vitrocom), which serve as sample chambers. Excess air is removed, and the cells are sealed to a microscope slide with fast-curing UV epoxy (Norland Products, NOA 81). For the time-dependent gelators, measurements begin immediately and are taken until the particle motion ceases. Data for the polyacrylamide samples is collected after 6 hours to ensure the reaction has equilibrated.

Samples are imaged using an inverted epifluorescence microscope (N.A. 1.2, 63× water-immersion objective, 1.0× tube lens, Axiovert 200, Zeiss). A high-speed CMOS camera (Phantom v5.1, Vision Research) is used to capture the motion of ~150 particles at 30Hz for a total of 800 frames. A weighted centroid method developed by Crocker and Grier (1996) is used to determine particle trajectories, from which the ensemble-averaged mean-squared displacement, $\langle \Delta r^2(\tau) \rangle$, is calculated. Sources of static error are accounted for by using a high-magnification immersion objective to increase the number of pixels per particle and remove background fluorescence, while dynamic error is reduced by using a short exposure time (σ=1000 μs) (Savin and Doyle, 2005).

3. Results and discussion

Mean-squared displacement (MSD)–Fig. 2 shows the ensemble-averaged mean-squared displacement versus lag time for the peptide (a) and polyacrylamide (c) systems. The MTHR peptide gel undergoes a time-dependent sol-gel transition; each curve is a measurement taken at 5 minute intervals after the self-assembly process is initiated. For the polyacrylamide, each curve represents a separate sample with increasing cross-linker concentration.

Let us examine the MSD curves in detail. At short gel times (peptide) and low cross-linker concentrations (acrylamide), the dynamics are consistent with probe particles that are free to diffuse as they sample a purely viscous environment, as indicated by $\langle \Delta r^2(\tau) \rangle \sim \tau$. As the polymer clusters grow, the viscosity of the solution increases, which decreases the magnitude of the MSD. Next, sub-diffusive dynamics emerge at short lag times, consistent with Rouse-like dynamics, followed by a broad cross-over to diffusive dynamics at long lag times. Eventually, the gel point is reached as the cross-linked network percolates the sample-

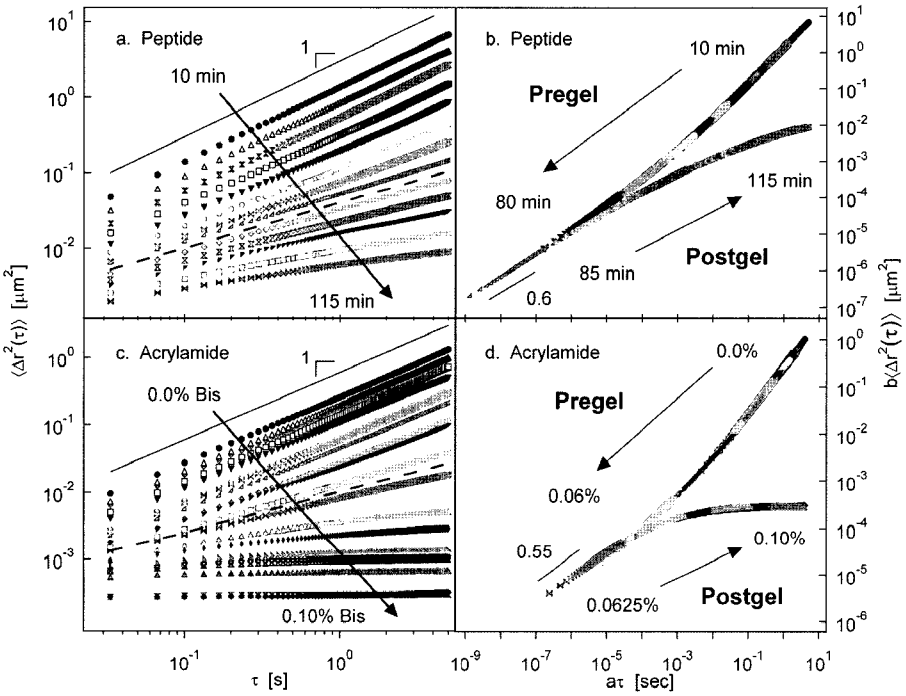

Fig. 2. Ensemble averaged mean-squared displacement $\langle \Delta r^2(\tau) \rangle$ of embedded polystyrene microspheres (D=1.05±0.01 μm) plotted versus lag time. Individual curves represent the particle dynamics at various extents of gelation. (a) Self-assembly of a 0.15 wt% peptide solution is initiated by the addition of buffer, and gelation proceeds with time, t, from 10-115 min. (b) Superposition of the peptide MSD data. (c) Gelation of equilibrated 3.0 wt% polyacrylamide gels with bis-acrylamide cross-linker concentrations from 0.0-0.10 wt%. (d) Superposition of the polyacrylamide MSD data. Dashed lines in (a) and (c) indicate the gel point and have logarithmic slopes of 0.6 and 0.55 for the peptide and polyacrylamide systems, respectively. Master curves in (b) and (d) are created before and after the gel point by shifting the data vertically, $b \cdot \langle \Delta r^2(\tau) \rangle$, and horizontally, $a \cdot \tau$, to account for changes in the MSD and longest relaxation time as the connectivity of the percolating network increases.

space and forms an incipient gel.

Beyond the gel point, continued gelation results in increasing connectivity, which forms a viscoelastic solid, as indicated by the onset of an elastic plateau at long lag times. While the Rouse-like sub-diffusive dynamics persist at short lag times with the same power-law scaling, the longest relaxation time continuously decreases, and the plateau extends to shorter lag times. At the longest times and highest cross-linker concentration, the thermal motion of the embedded particles is completely arrested by the gel network.

Gel point and critical behavior–As noted earlier, the gel point and critical scaling exponents can be found using the principles of time-cure superposition (Adolf and Martin, 1990). Individual MSD curves are multiplied by a time shift factor a and an MSD shift factor b to construct pre- and postgel master curves shown in Fig. 2(b) and (d). Shifting for the pregel curve begins at the lowest extent of gelation, where the particle dynamics are diffusive, and continues until curves can no longer be successfully superimposed. After this point, a second postgel curve begins at the highest extent of gelation, where particle motion is arrested by the elastic gel network, and continues until the final MSD curve near the gel point is added. The resulting master curves converge and exhibit a common logarithmic slope $\alpha = d\ln\langle\Delta r^2(\tau)\rangle / d\ln\tau$, which, in the case of the systems shown here, is between $0.55 \le \alpha \le 0.6$.

In Fig. 3 we show the reciprocal time and MSD shift factors, a^{-1} and b^{-1}, as a function of time, t, or cross-linker concentration, p, for the MTHR peptide and polyacrylamide systems, respectively. The reciprocal shift factors for both branches of the master curve increase asymptotically. This is expected: a^{-1} reflects the divergence of the longest relaxation time τ_L, while b^{-1} captures the divergence of the steady-state creep compliance J_e^0 (Adolf and Martin, 1990; Joanny, 1982; Winter and Mours, 1997). The resulting asymptote identifies the gel point, marked by the dashed lines in Fig. 3. The gel point for 0.15 wt% peptide is $t_c = 82$ minutes, while the gel point for 3.0 wt% polyacrylamide is $p_c = 0.062$ wt% bis-acrylamide.

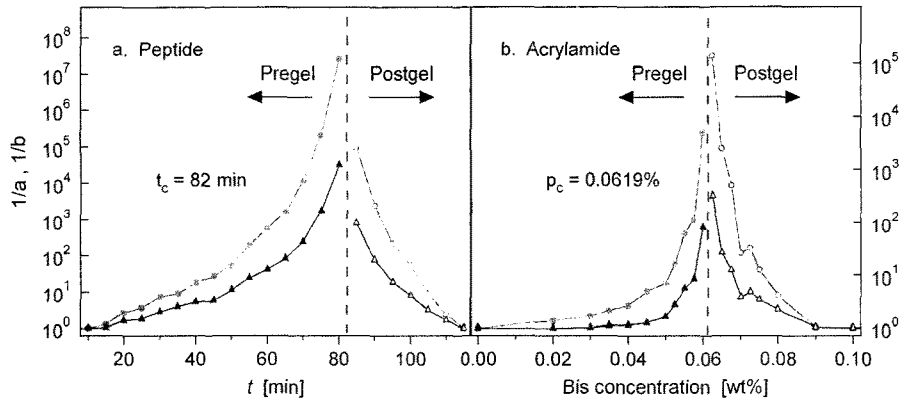

Fig. 3. The reciprocal of the shift factors a (circles) and b (triangles) used for superposition in Fig. 3 are plotted as a function of self-assembly time, t, for (a) the peptide hydrogel and (b) as a function of cross-linker concentration for the polyacrylamide gels. The critical gel point, t_c or p_c, is determined by the asymptotic behavior, illustrated by the dashed vertical line.

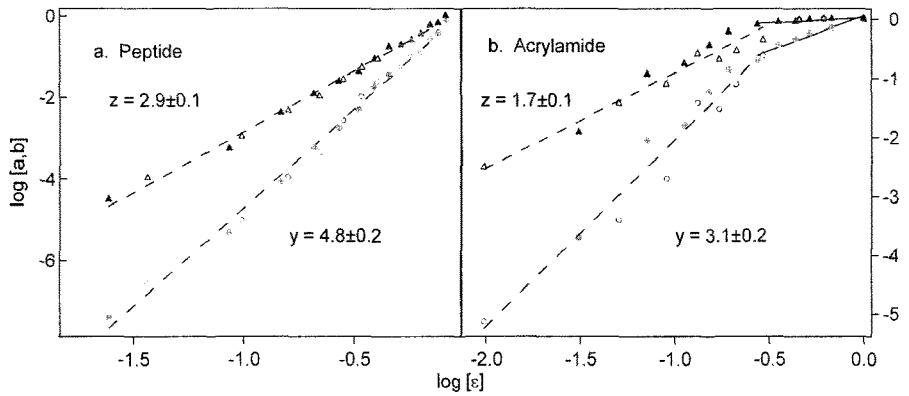

Fig. 4. Shift factors a (circles) and b (triangles) are plotted versus the distance from the gel point, ε, for (a) MTHR peptide and (b) polyacrylamide. Solid symbols are for the pregel and open symbols are for the postgel. Dashed lines are linear fits of the logarithmic data with the corresponding dynamic scaling exponents shown. The solid lines at high values of ε in for the polyacrylamide have slope 0.2 ± 0.1 (upper curve) and 1.2 ± 0.1 (lower curve).

With the gel point identified, we next define the distance from the gel point, $\varepsilon \equiv |p-p_c|/p_c$. Recall that the longest relaxation time and creep compliance are expected to exhibit power-law behavior, $\tau_L = \varepsilon^{-y}$ and $J_e^0 = \varepsilon^{-z}$ (Adolf and Martin, 1990). We can now calculate the scaling exponents y and z.

Fig. 4 shows a and b versus ε. We indeed observe the expected power law behavior. For the peptide system, the power law is well-defined for the observed range $0.03 \leq \varepsilon \leq 1$. Since a and b are inversely proportional to τ_L and J_e^0, the slopes of the lines shown in Fig. 4 give the critical exponents y and z for both the pre- and postgels. In both systems, there is excellent agreement between the scaling exponents found for the pregel and postgel. The scaling exponents determined for the MTHR peptide are $y = 4.8 \pm 0.2$ and $z = 2.9 \pm 0.1$ while those for the polyacrylamide gel are $y = 3.1 \pm 0.1$ and $z = 1.7 \pm 0.1$. These values are consistent with those predicted for the percolation universality class, in which $y = 4$ and $z = 8/3$, assuming the hydrodynamic screening of Rouse dynamics (Martin *et al.*, 1988). In contrast, the exponents predicted from Zimm theory (unscreened hydrodynamic interactions) are $y = 8/3$ and $z = 8/3$ (Martin *et al.*, 1988), and de Gennes' electrical network analogy leads to $y = 2.69$ and $z = 1.94$ (Derrida *et al.*, 1983).

We now examine the polyacrylamide data in more detail, noting that the shift factors for this system exhibit significantly more noise than the peptide, as well as a deviation from the expected power-law behavior at higher values of ε. A significant contributor of noisy data is the inherent uncertainty in the extent of reaction that comes with making many samples. We find that degassing the samples prior to use is a critical step in the sample preparation, indicating the sensitivity of the free-radical polymerization reaction to environmental and preparation conditions.

The deviation from the power law exponent in the polyacrylamide data shown in Fig. 4(b) between $0.3 \leq \varepsilon \leq 1$ is more interesting, and highlights a subtle issue in the time-cure superposition analysis. In this range of ε, the time shift factor appears to scale with a lower power law exponent, as indicated by the solid line in the figure with slope 1.2 ± 0.1. This represents a limitation in the time-cure superposition analysis of microrheological data: accurate superposition of both time and compliance are only possible when the longest relaxation time is in the vicinity of the window of lag times over which the probe particle dynamics are sampled in the experiment. Consider the initial stages of polymerization. As large molecules form, the viscosity will increase (the expected dependence is $\eta_0 \sim \varepsilon^{-k}$). Correspondingly, the mean-squared displacement will decrease. This is because the compliance is related to both the viscosity and longest relaxation time by $J_e^0 \sim \tau_L/\eta_0$. However, if $\tau_L \ll \tau_{\min}$, where $\tau_{\min}$ is the shortest lag time of the particle tracking, the shift of the MSD curve will be ambiguous. One could shift the next MSD curve either in time (along the abscissa) or in MSD (along the ordinate). In the latter case, the shift factor will be $b' \sim \varepsilon^k$ instead of the expected $b' \sim \varepsilon^{y-k}$, where $z = y - k$. Because the MSD is diffusive for $\tau \gg \tau_L$ (thus, $\langle \Delta r^2(\tau) \rangle \sim \tau$), the same shift value is obtained if the MSD is shifted along the abscissa. This is the case shown in Fig. 4(b). Indeed, the power law exponent in this range of ε is close to $y - z = 1.4$, and the corresponding MSD shift is negligible in the same region. Without information with regard to the longest relaxation timescale, the data should be shifted along the ordinate, which reflects the increasing viscosity of the polymerizing solution. However, this can only be done in the case of purely diffusive probe dynamics when $\tau \gg \tau_L$.

Finally, the critical relaxation exponent, n, can be calculated from the dynamic scaling exponents, using the relationship $n = z/y$ (Adolf and Martin, 1990). The critical scaling exponents for the MTHR peptide and polyacrylamide hydrogels are $n = 0.60 \pm 0.02$ and $n = 0.55 \pm 0.03$, respectively, which is in agreement with Rouse dynamics of fractal clusters, for which $n = 2/3$. Furthermore, the calculated critical exponents are consistent with the slope of the MSD curves close to the gel transition point. We compare the critical relaxation exponent to the MSD for polyacrylamide in Fig. 5. Closest to the gel point, the curves obey nearly power-law behavior. Identical power-law dynamics can be observed in MSD curves further from the gel point at short lag times, reflecting the shorter relaxation time of the polymer clusters (in the pregel) or polymer network (in the postgel). In the pre-gel, the initial power-law

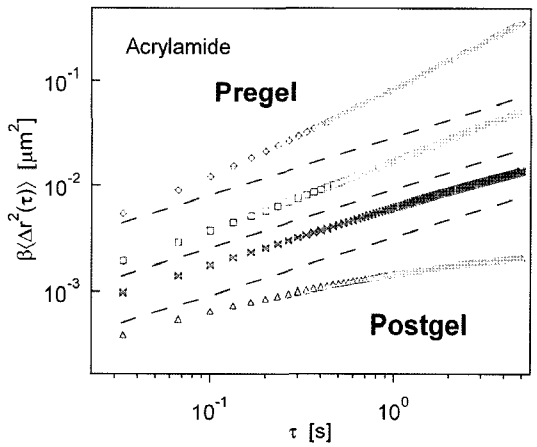

Fig. 5. MSD curves from Fig. 2c for 3.0 wt% polyacrylamide gels near the critical gel point. The gel point corresponds to frequency-independent power-law scaling of the creep compliance, where the dashed lines indicate a slope $\alpha = 0.55$. Before the gel point, subdiffusive behavior is seen at short times, while relaxation towards diffusion occurs at long lag times. After the gel point, an elastic plateau emerges, characteristic of a viscoelastic solid.

crosses over to diffusive dynamics, while in the post-gel, the same power-law crosses over to arrested dynamics.

4. Application to other systems

HMWH-PEG hydrogels–Another hydrogel system we have studied consists of malemide functionalized high molecular weight heparin (HMWH) as a backbone polymer that is cross-linked with dithiolized poly(ethylene glycol) (PEG). In contrast to the previous peptide and acrylamide gels, this system is similar to a vulcanization type gelation process, but in the dilute regime. For lower maleimide functionalities (~4), we measure the material rheology as a function of gel time.

As shown in Fig. 6, analyzing the HMWH-PEG hydrogels with time-cure superposition yields trends that are similar to those found in the previous hydrogel systems. Fig. 6 captures the kinetically evolving hydrogel system, measuring the growth of the percolating network until an elastic solid is formed. Master curves, created by shifting the MSD along the ordinate and abscissa are again created. The network in this case exhibits a gel point close to 45 minutes after the precursors are mixed. Interestingly, the critical relaxation exponent, determined from the MSD logarithmic slope at short scaled lag times is $n \approx 0.4$. Measurements are also taken along a constant total weight percent line in the hydrogel system (data not shown), and the critical relaxation exponents remain constant, suggesting that the structure of the hydrogel is independent of the heparin to PEG ratio.

The critical relaxation exponent value is lower than those reported for the peptide and acrylamide systems. This possibly reflects the different structure of the gelling material, which may be expected given the much larger molecular weights of the precursor molecules. The value of n is consistent with a mean-field universality class (Stauffer *et al.*, 1982). Typically, this class is observed when the molecular weight between cross-links is high.

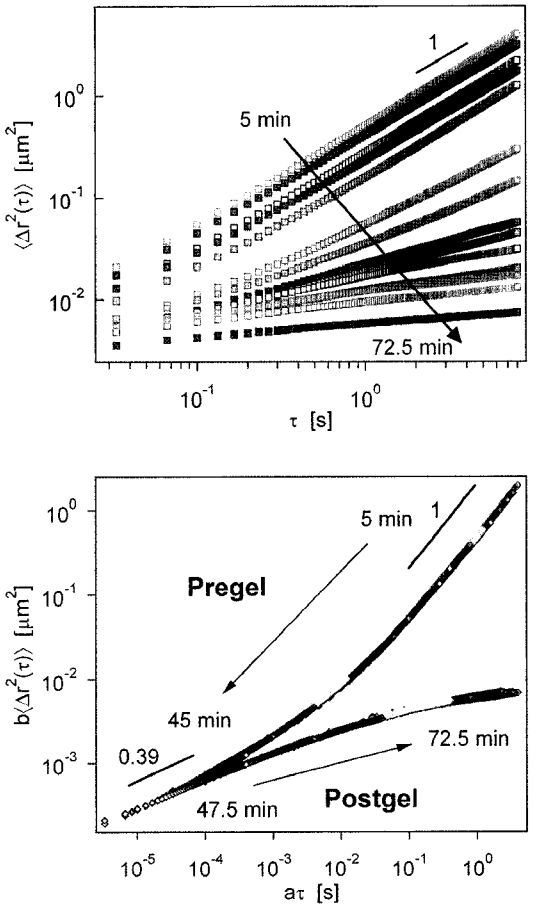

Fig. 6. 2.86 wt% HMWH, 2.12 wt%PEG gel (1× PBS buffer, pH 7.4, T=25C). (Top) MSD versus lag time. (Bottom) Superposition of the HMWH-PEG MSD data. Both master curves have a logarithmic slope of ~0.4 at low values of $a\tau$.

5. Conclusions

In this work, we presented a survey of recent results on the microrheology of the liquid-solid transition. Our studies demonstrated that microrheology is capable of extracting the full spectrum of rheological information near the gel point, including the critical extent of reaction (by the identification of the gel point), the critical relaxation exponent, and other critical dynamic scaling exponents. It is encouraging that microrheology can be used with the same apparent rigor that bulk rheological methods have provided over the past two decades.

Microrheology will be unlikely to *replace* bulk rheological methods in their entirety, nor should that be our aim or expectations. Rather, microrheology *complements* macrorheological characterization by providing rheological information for samples that would otherwise be difficult or impossible to study using bulk rheology. The fast gelation kinetics and weak incipient structures of many hydrogelators (or similar gelators operating at high solvent dilution) are ideal candidates. Similarly, the biomaterials that we studied here are scarce and expensive; microrheology is advantageous because of the small sample size requirements compared with bulk rheology.

Many questions remain. The application of single-point microrheology techniques, like those employed in this paper, will limit studies to materials without significant microheterogeneities or nanoscale structure near the probe particles that cause violations of the generalized Stokes-Einstein relationship. It will be important to verify whether the methods described here can be extended to two-point microrheology, and under what conditions two-point will be necessary.

Acknowledgments

We thank J. Schneider and K. Rajagopal for providing peptide samples, K. Kiick and A. Baldwin for providing HMWH-PEG samples and P. Spicer for stimulating discussions. Funding for this work was provided by the National Institutes of Health (1 R01 EB003172-01 and 2 P20 016472-04) and the Procter and Gamble Company.

References

Adolf, D. and J. E. Martin, 1990, Time cure superposition during cross-linking, *Macromolecules* **23**, 3700-3704.

Bobroff, N., 1986, Position measurement with a resolution and noise-limited instrument, *Rev. Sci. Instrum.* **57**, 1152-1157.

Chin, K. and J. P. Vacanti, 2008, Hydrogel-perfluorocarbon composite scaffold promotes oxygen transport to immobilized cells, *Biotech. Prog.* **24**, 358-366.

Crocker, J. C. and D. G. Grier, 1996, Methods of digital video microscopy for colloidal studies, *J. Coll. Int. Sci.* **179**, 298-310.

Davis, M. E., J. P. M. Motion, D. A. Narmoneva, T. Takahashi, D. Hakuno, R. D. Kamm, S. G. Zhang and R. T. Lee, 2005, Injectable self-assembling peptide nanofibers create intramyocardial microenvironments for endothelial cells, *Circulation* **111**, 442-450.

Davis, M. W. and J. P. Vacanti, 1996, Toward development of an implantable tissue engineered liver, *Biomaterials* **17**, 365-372.

Derrida, B., D. Stauffer, H. J. Herrmann and J. Vannimenus, 1983, Transfer-matrix calculation of conductivity in 3-dimensional random resistor networks at percolation-threshold, *J. Phys. Lett. (France)* **44**, L701-L706.

Ellis-Behnke, R. G., Y. X. Liang, S. W. You, D. K. C. Tay, S. G. Zhang, K. F. So and G. E. Schneider, 2006, Nano neuro knitting: peptide nanofiber scaffold for brain repair and axon regeneration with functional return of vision, *Proc. Natl. Acad. Sci. USA* **103**, 5054-5059.

Ferry, J., 1980, *Viscoelastic properties of polymers*, Wiley, New York.

Gardel, M. L., M. T. Valentine, J. C. Crocker, A. R. Bausch and D. A. Weitz, 2003, Microrheology of entangled F-actin solutions, *Phys. Rev. Lett.* **91**, 158302.

Grinstaff, M. W., 2007, Designing hydrogel adhesives for corneal wound repair, *Biomaterials* **28**, 5205-5214.

Haines-Butterick, L., K. Rajagopal, M. Branco, D. Salick, R. Rughani, M. Pilarz, M. S. Lamm, D. J. Pochan and J. P. Schneider, 2007, Controlling hydrogelation kinetics by peptide design for three-dimensional encapsulation and injectable delivery of cells, *Proc. Natl. Acad. Sci.* **104**, 7791-7796.

Hoffman, A. S., 2002, Hydrogels for biomedical applications, *Adv. Drug Delivery Rev.* **43**, 3-12.

Joanny, J. F., 1982, Flow birefringence at the sol-gel transition, *J. Phys. (France)* **43**, 467-473.

Langer, R. and N. A. Peppas, 2003, Advances in biomaterials, drug delivery, and bionanotechnology, *AIChE J.* **49**, 2990-3006.

Larsen, T. H. and E. M. Furst, 2008, Microrheology of the liquid-solid transition during gelation, *Phys. Rev. Lett.* **100**, 146001.

Lee, K. and D. J. Mooney, 2001, Hydrogels for tissue engineering, *Chem. Rev.* **101**, 1869-1879.

Lutolf, M. P. and J. A. Hubbell, 2005, Synthetic biomaterials as instructive extracellular microenvironments for morphogenesis in tissue engineering, *Nat. Biotechnol.* **23**, 47-55.

Martin, J. E., D. Adolf and J. P. Wilcoxon, 1988, Viscoelasticity of near-critical gels, *Phys. Rev. Lett.* **61**, 2620-2623.

Martin, J. E., D. Adolf and J. P. Wilcoxon, 1989, Viscoelasticity near the sol-gel transition, *Phys. Rev. A* **39**, 1325-1332.

Mason, T. G., 2000, Estimating the viscoelastic moduli of complex fluids using the generalized Stokes-Einstein equation, *Rheol. Acta* **39**, 371-378.

Mikos, A. G., S. W. Herring, P. Ochareon, J. Elisseeff, H. H. Lu, R. Kandel, F. J. Schoen, M. Toner, D. Mooney, A. Atala, M. E. Van Dyke, D. Kaplan and G. Vunjak-Novakovic, 2006, Engineering complex tissues, *Tissue Engineering* **12**, 3307-3339.

Nie, T., A. Baldwin, N. Yamaguchi and K. L. Kiick, 2007, Production of heparin-functionalized hydrogels for the development of responsive and controlled growth factor delivery systems, *J. Controlled Release* **122**, 287-296.

Ozbas, B., J. Kretsinger, K. Rajagopal, J. P. Schneider and D. J. Pochan, 2004, Salt-triggered peptide folding and consequent self-assembly into hydrogels with tunable modulus, *Macromolecules* **37**, 7331-7337.

Palmer, A., J. Y. Xu and D. Wirtz, 1998, High-frequency viscoelasticity of crosslinked actin filament networks measured by diffusing wave spectroscopy, *Rheol. Acta* **37**, 97-106.

Peppas, N. A., P. Bures, W. Leobandung and H. Ichikawa, 2000, Hydrogels in pharmaceutical formulations, *Eur. J. Pharmacol. Biopharm.* **50**, 27-46.

Pochan, D., J. P. Schneider, J. Kretsinger, B. Ozbas, K. Rajagopal and L. Haines, 2003, Thermally reversible hydrogels via intramolecular folding and consequent self-assembly of a de Novo designed peptide, *J. Am. Chem. Soc.* **125**, 11802-11803.

Rajagopal, K. and J. P. Schneider, 2004, Self-assembling peptides and proteins for nanotechnological applications, *Curr. Opin. Struct. Biol.* **14**, 480-486.

Savin, T. and P. S. Doyle, 2005, Static and dynamic errors in particle tracking microrheology, *Biophys. J.* **88**, 623-638.

Savin, T. and P. S. Doyle, 2007, Electrostatically tuned rate of peptide self-assembly resolved by multiple particle tracking, *Soft Matter* **3**, 1194-1202.

Scanlan, J. C. and H. H. Winter, 1991, Composition dependence of the viscoelasticity of end-linked poly(dimethylsiloxane) at the gel point, *Macromolecules* **24**, 47-54.

Schneider, J. P., D. J. Pochan, B. Ozbas, K. Rajagopal, L. Pakstis and J. Kretsinger, 2002, Responsive hydrogels from the intramolecular folding and self-assembly of a designed peptide, *J. Am. Chem. Soc.* **124**, 15030-15037.

Stauffer, D., A. Coniglio and M. Adam, 1982, Gelation and critical phenomena, *Adv. Polym. Sci.* **44**, 103-158.

Stevens, M. M. and J. H. George, 2005, Exploring and engineering the cell surface interface, *Science* **310**, 1135-1138.

Tseng, Y., K. M. An and D. Wirtz, 2002, Microheterogeneity controls the rate of gelation of actin filament networks, *J. Biol. Chem.* **277**, 18143-18150.

Veerman, C., K. Rajagopal, C. S. Palla, D. J. Pochan, J. P. Schneider and E. M. Furst, 2006, Gelation kinetics of beta-hairpin peptide hydrogel networks, *Macromolecules* **39**, 6608-6614.

Winter, H. H. and F. Chambon, 1986, Analysis of linear viscoelasticity of a cross-linking polymer at the gel point, *J. Rheol.* **30**, 367-382.

Winter, H. H. and F. Chambon, 1987, Linear viscoelasticity at the gel point of a cross-linking PDMS with imbalanced stoichiometry, *J. Rheol.* **31**, 683-697.

Winter, H. H. and M. Mours, 1997, Rheology of polymers near liquid-solid transitions, *Adv. Polym. Sci.* **134**, 165-234.

Wu, D. Q., Y. X. Sun, X. D. Xu, S. X. Cheng, X. Z. Zhang and R. X. Zhuo, 2008, Biodegradable and pH-sensitive hydrogels for cell encapsulation and controlled drug release, *Biomacro.* **9**, 1155-1162.

Xu, C. Y., V. Breedveld and J. Kopecek, 2005, Reversible hydrogels from self-assembling genetically engineered protein block copolymers, *Biomacro.* **6**, 1739-1749.

Zimenkov, Y., S. N. Dublin, R. Ni, R. S. Tu, V. Breedveld, R. P. Apkarian and V. P. Conticello, 2006, Rational design of a reversible pH-responsive switch for peptide self-assembly, *J. Am. Chem. Soc.* **128**, 6770-6771.